Research Article

Tidal dynamics drive ooid formation in the Capricorn Channel since the Last Glacial Maximum

Katherine C. Lee [a,*], Jody M. Webster [b], Tristan Salles [b], Eleanor E. Mawson [a,c,d], Jon Hill [a]

[a] Department of Environment and Geography, University of York, UK
[b] Geocoastal Research Group, School of Geosciences, The University of Sydney, Sydney, New South Wales, Australia
[c] The Lyell Centre, Heriot-Watt University, Edinburgh, Scotland, UK
[d] Engineering and Physical Sciences, Heriot-Watt University, Edinburgh, Scotland, UK

ABSTRACT

Relative sea-level changes can dramatically alter coastal geomorphology and coastlines, which, in turn, can fundamentally alter tidal regimes. The Great Barrier Reef (GBR) has undergone around 120 m of relative sea level (RSL) rise since the Last Glacial Maximum, ~20,000 years ago (ka). Ooid grains (sand sized carbonate sediment) that formed in shallow water (>5 m depth) and under prolonged hydrodynamics forcing are now found at depth ranging between 100 and 120 m under the present day GBR Gulf of Capricorn. The apparent inconsistency between preferential conditions for their formation and the actual environment where they are found at present-day could be used to infer past regional hydrodynamic conditions. Here, we focus on the regional changes in the GBR tidal dynamics over the last 16.8 ka to show that sea-level rise on the GBR has caused significant changes on tidal patterns and dynamics. To do so, we used the first multi-scale palaeo-tidal finite element coastal tidal model of the GBR over five time slices (present day, ~10 ka, ~12 ka, ~15 ka and 16.8 ka), representing the position of RSL at 0 m, 20 m, 45 m, 75 m and 96 m below present. We show that favourable conditions for ooid formation only existed for a short period of time between 16.8 and 11 ka. At that time, the Gulf of Capricorn was a wide shallow shelf with strong currents constantly agitating grains, providing rapid burial, exposure and re-burial cycles. We show that these conditions only existed for a short period of time and hence explain the presence of ooid grain formation in the GBR at that time. We propose ooids formed within the Capricorn Channel at a time of lower RSL than expected and then underwent sub-tidal transportation to their final deposition place via tidal currents, explaining the inconsistency with their age and the depth at which they were found.

1. Introduction

The modern GBR is the world's largest reef, sitting on the 120 km continental shelf edge of north-eastern Australia (Hinestrosa et al., 2016; King and Wolanski, 1996; Wolanski, 1983). Average depth of the inner shelf is 20 m, increasing to ~100 m near the shelf edge and then steeply decreasing over 1500 m after the shelf break (Wolanski, 1983). Reefs sit higher than the seabed and tend to be exposed, generating cross-shore gradients in radiation stress, creating complex paths for tides to navigate through (Andutta et al., 2012; Taebi et al., 2011). Tides on the GBR are controlled by the Coral Sea and are primarily influenced by shelf bathymetry and dominant tidal constituents M2, O1, N2, K1 and S2 (Wolanski, 1983). These five constituents are responsible for 87.5% of the tidal variation in relative sea level (RSL) at Townsville, Queensland;

the most significant of which is M2, being a factor of two greater in magnitude than the other constituents (Andrews and Bode, 1988). The GBR is subjected to a large spring and neap tide cycle (up to 87% difference between neap and spring cycles) which are each steered very differently by reef density, leading to individual complex tidal phenomena between each oscillation (Mawson et al., 2022; Wolanski, 1983).

1.1. Ooid grains

Ooids are spherical or ovoidal carbonate grains with diameters ranging from 0.1 to 2.0 mm (Simone, 1980; Diaz and Eberli, 2019). They typically form in specific tropical oceanic conditions at depths no deeper than five metres, with strong current action continuously agitating the

seabed, along with well-defined chemical properties (Yokoyama et al., 2006; Mackenzie and Pigott, 1981; Diaz and Eberli, 2019). To form they require warm water chemically supersaturated in calcium carbonate with a source of nuclei and constant agitation (Diaz and Eberli, 2019; Loreau and Purser, 1973; Reeder and Rankey, 2008). High pH and high alkalinity are thought to be key in creating the right chemical environment (Rankey and Reeder, 2009), such as the present day Bahamas (Newell et al., 1960). Microbial activity is also thought to play a part in formation of the grains via biomediation (Diaz and Eberli, 2019). Newly formed ooids are aragonite or magnesium-calcite, and are converted to calcium carbonate over time (Taylor and Illing, 1969). Ooids were initially found in the GBR in 1970 via small pipe dredges at the mouth of the Capricorn Channel (CC) in an area of 340 km^2 (Fig. 1), were 0.1–0.3 mm in size, spherical/ellipsoidal/discoidal in shape, well polished and composed of high magnesium calcite (Marshall and Davies, 1975). This study is focusing on an area containing seven sites which were found with >3% of ooid grains, all of which are situated on the edge of the CC mouth. Although ooids have been found at Lizard Island (Davies and Martin, 1976), the apparent lack of ooids elsewhere in the GBR is rather surprising, as the GBR corresponds to one of the largest areas of carbonate production with chemical conditions considered ideal for ooid development (Marshall and Davies, 1975). Previous work hypothesised that oceanic conditions were favourable at that time for microbialite formation, for example, at ~12 ka carbonate accumulation increased, potentially influenced by a difference in seawater pH due to changes in environmental conditions, such as lower RSL positions taking place between 30 ka and 10 ka (Szilagyi et al., 2020). In this study we assume that the chemical and biological conditions were suitable for the formation of ooid grains, as we focus on the physical conditions present. No study has yet been able to explain how ooids formed in the GBR, as the necessary physical conditions do not exist at present (Yokoyama et al., 2006).

1.2. Tidal dynamics of the Great Barrier Reef

Past literature has suggested that from 17 ka onwards, there have been large variations in RSL associated with the depletion of ice sheets since the Last Glacial Maximum (LGM) (Lambeck et al., 2014; Webster et al., 2018; Yokoyama et al., 2006), leading to an estimated 97 m RSL rise since 17 ka (Yokoyama et al., 2006). Previous studies have shown GBR tides are extremely sensitive to spatial heterogeneity, caused by reef matrices and changes in bathymetry, affecting hydrodynamics and tidal circulation through reefs (King and Wolanski, 1996; Taebi et al., 2011). As RSL rose over the past 17 ka, causing coastal resculpting, it would be expected that tidal patterns would change (Harker et al., 2019; Hinestrosa et al., 2016).

The ooid finding inconsistency is as follows: although the ooid samples were collected from the sea bed 100–120 m below RSL, the ooids were aged 16,800 ka which is when RSL was 96 m below present day: for ooids to be formed at the depth found, the ooids would need to be ~ 24,000 years old (Yokoyama et al., 2006). Given the sensitivity of GBR tides to RSL change, the tidal currents at 16.8 ka would be expected to be significantly different to the present day and hence may explain formation of ooid grain at the particular time. In order for ooids to form in the GBR, the physical conditions should be: an average depth of ~5 m, increased tidal velocity of at least ~0.7 m/s and increased tidal range to allow constant agitation in the ooid area (Reeder and Rankey, 2008). A possibility of how the grains were deposited there is that grains were transported from a shallower place of formation to the CC, however this was considered unlikely due to present day velocity measurements
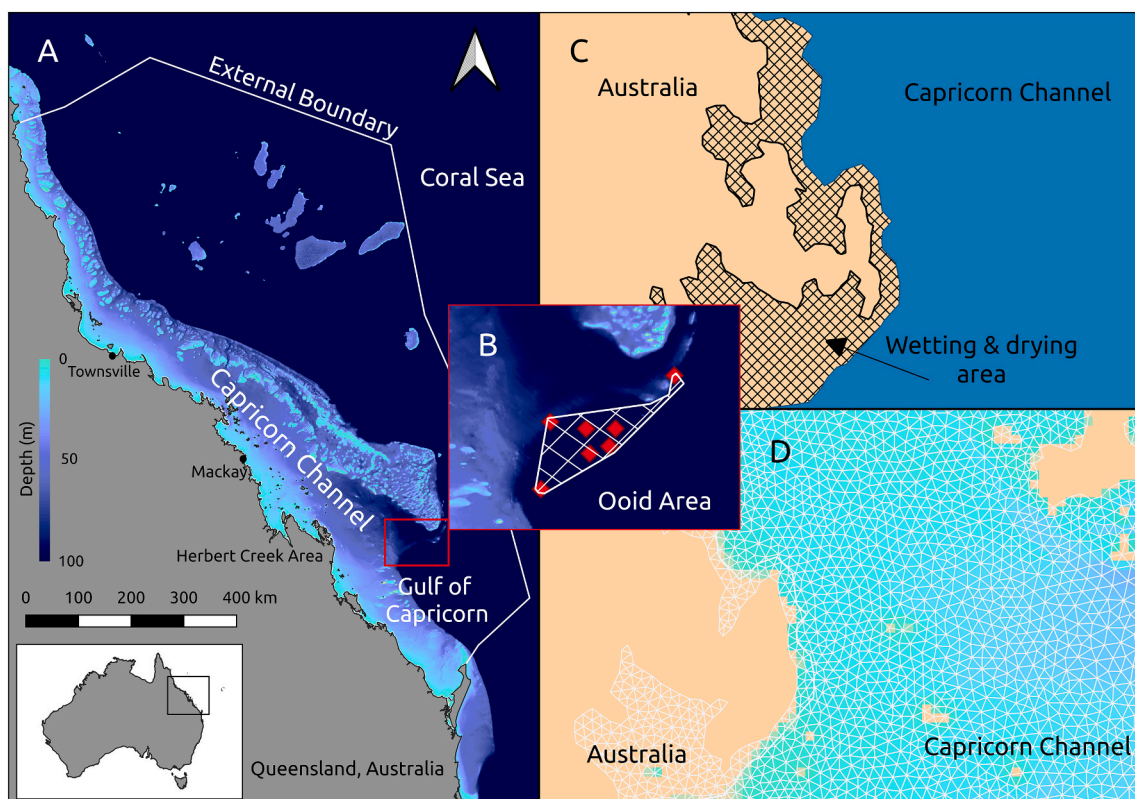
Fig. 1. A) map of model bathymetry and model domain showing key areas and location of ooid findings. B) zoom-in of the area ooids were found. Squares indicate precise location of samples taken, with the hatched area depicting the area enclosed by samples containing >3% ooids C) zoom-in area of model domain illustrating the land (orange), wetting and drying (hatched) and coastal boundaries (blue-orange boundary). D) zoom-in area of model domain showing the high resolution mesh (white lines) over bathymetry (blue shading). Note the mesh extends onto the land (orange) to facilitate the calculation of wetting and drying. (For interpretation of the references to colour in this figure legend, the reader is referred to the web version of this article.)

(Yokoyama et al., 2006).

Due to GBR tidal systems and bathymetric complexities, only numerical modelling is currently capable of constructing a realistic palaeogeographic tidal model to conduct a study into palaeo-tidal history (Collins et al., 2017, 2021). In reef areas wetting and drying calculations are crucial: during high tide, currents will go over/through the submerged reef matrices whereas during low tide, currents will go around exposed reefs (Seifi et al., 2019). This results in different distributions of sediment from different patterns of bed shear stress, induced by local morphological variations and related to changes in the composition and resistance of bed sediment. Sensitivities such as those found on the GBR means that coarse resolution or missed bathymetric structures or complexities could lead to inaccurate assumptions (Harker et al., 2019; Seifi et al., 2019). As representing bottom bathymetry is important to the study, numerical models developed for this purpose need mesh resolution fine enough to capture bathymetric influences of the reefs while simulating hydrodynamic phenomena experienced on the GBR (King and Wolanski, 1996; Seifi et al., 2019). In this study we use a resolution of 500 m in order to capture important bathymetry features across the entire GBR area. Five unstructured meshes are created to run with Thetis (Kärnä et al., 2018) and will represent the modern day bathymetry and then −20 m, −45 m, −75 m and − 96 m of RSL reduction corresponding to 10 ka, 12.5 ka, 15 ka and 16.8 ka respectively (Fig. 2).

2. Methods and materials

2.1. Thetis

Thetis (Kärnä et al., 2018) is used to create the first palaeo-tidal numerical model for the GBR. Thetis was chosen for its capacity for multi-scale high resolution, tidal accuracy as well as its ability to solve non-linear shallow water equations, bed shear stress and wetting and drying (Goss et al., 2019; Harker et al., 2019; Kärnä et al., 2018). To support the hypothesis that a different set of tidal patterns and
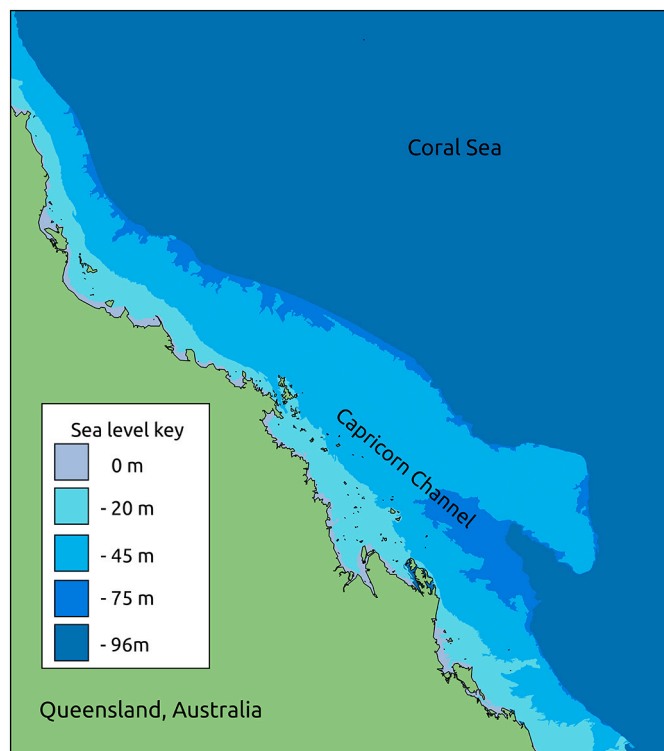

Fig. 2. Illustration of the modern day coastline and sea level against the four palaeo sea levels.

conditions existed in the southern GBR at 16.8 ka allowing for ooid grains formation, the study is looking at whether there were significant differences in palaeo tides compared to present day and whether those conditions could form ooids. The tidal currents and dynamics will be analysed across the whole GBR, but focusing on the Gulf of Capricorn (GoC)where the ooid grains were found, to determine if tidal dynamics were favourable for ooid formation.

Numerical models that represent coastal ocean regions can be used to predict the altered hydrodynamics caused by tides. Thetis (Kärnä et al., 2018) is a finite element model used to solve 2D and 3D depth averaged models as well as solving non-conservative nonlinear shallow water equations which can be expressed using eqs. 1 and 2 (Angeloudis et al., 2018). We employ Thetis as a 2D flow solver for simulating coastal flows, implemented using Firedrake finite element Partial Differential Equation solver framework which is also capable of performing wetting and drying calculations (Goss et al., 2019; Kärnä et al., 2018).

$$\frac{\partial \eta}{\partial t} + \nabla \cdot (H\mathbf{u}) = 0, \tag{1}$$

$$\frac{\partial \mathbf{u}}{\partial t} + \mathbf{u} \cdot \nabla \mathbf{u} + f\mathbf{u}^\perp + g\nabla\eta = -\frac{\tau_b}{\rho H} + \nabla\left(\nu\left(\nabla\mathbf{u} + \nabla\mathbf{u}^T\right)\right), \tag{2}$$

where η is the free surface height, H is the total water depth given by $H = \eta + h$ where h is the bathymetry, ν is the kinematic viscosity of the fluid, and $\mathbf{u}$ is the depth-averaged velocity vector. The Coriolis term is represented as $f\mathbf{u}^\perp$, where $\mathbf{u}^\perp$ the velocity vector rotated counter-clockwise over 90°. In turn, $f = 2\Omega \sin \zeta$ with Ω corresponding to the angular frequency of the Earth's rotation and ζ the latitude. Bed shear stress (τ_b) effects are represented through the Manning's n formulation as:

$$\frac{\tau_b}{\rho} = gn^2 \frac{|\mathbf{u}|\mathbf{u}}{H_d^{\frac{1}{3}}} \tag{3}$$

where n is the Manning's friction coefficient. The model is implemented using a discontinuous Galerkin finite element discretisation (DG-FEM), using the $P_{1DG} - P_{1DG}$ velocity-pressure finite element pair.

2.2. Mesh generation

Five tidal models were made for the analysis of palaeo-tides of the GBR. These models extend from the central to the southern GBR lagoon with particular focus on the GoC where ooids were found. The models consisted of the present day RSL used for model validation and then four palaeo tidal simulations.

QGIS 3.12 (QGIS.org, 2020) was used to define meshed domains which were then converted to a suitable format for meshing via *qmesh* (Avdis et al., 2018). In order to derive the necessary 2D data required, bathymetric information was extracted from GBR100 (Beaman, 2010). To construct the paleo-bathymetry, we modified the present-day GBR100 DEM (digital elevation model) (Beaman, 2010) to first remove Holocene terrigenous sediment accumulation along the coast and the inner shelf assuming an average 7.5 m deposition along the coastline at around the 15 m isobath, tapering to 0 m at the coast and at the 25 m isobath (Maxwell and Swinchatt, 1970; Salles et al., 2018). The paleo-surface is then further refined by removing the average thickness of the Holocene reefs. Details of reef cores reaching the Pleistocene surface in the GBR show variations in reef thicknesses from 5 to 25 m (Marshall and Davies, 1984; Webster and Davies, 2003; Hinestrosa et al., 2022). To remove the Holocene coral reefs, we used the modern reef positions (Hopley et al., 2007) and removed estimated Holocene coral reef thicknesses in these locations. From this, QGIS was used to extract a 10 m contour to use as a 'coastline' boundary which allows for the wetting and drying calculations (Fig. 1). Once the contour was extracted, small islands under 1000 m in length were removed from the domain, followed by enlarging or removing inlets under the width of

500 m as well as islands intersecting boundaries, all of which would cause erroneous geometries such as oscillations resulting in instability (Avdis et al., 2018).

To represent RSL reduction in the palaeo models, QGIS was used to increase the bathymetry height in relation to each run, i.e., a bathymetric rise of 96 m for the model representing 96 m RSL position (Felis et al., 2022). For each mesh the same external/forced boundary was used with only minor edits to take into account intersections from revealed topography, as previous work found that moving the exterior boundary further away does not affect validation results (Martin-Short et al., 2015). This step investigates bathymetric changes, which refers to the bathymetry after removing the Holocene reefs and changing the RSL.

To convert the boundaries generated in QGIS for mesh generation, qmesh (Avdis et al., 2018) was used. All meshes were generated in UTM56S coordinate reference system and contain a maximum of 1,366,562 triangular elements and 681,892 nodes. A Delaunay triangulation algorithm was used in Gmsh (Geuzaine and Remacle, 2009) to create each mesh, with mesh resolution controlled by depth and distance from boundaries (Fig. 1). In other studies, a resolution of 150 m was used to investigate localised reef areas of 10×10 km square (Andutta et al., 2012) and a resolution of > 2 km was used to capture tidal movement of the whole of Australia (Harker et al., 2019). Here, the largest element size is 5 km, at a distance of 50 km from any boundary. The coastline boundary has a minimum edge length of 500 m to a distance of 1.5 km away, where the edge length increases linearly to the maximum 5 km when 50 km away. Similarly, the exterior boundary increased from 2.5 km resolution to 6 km away from the boundary. In addition, depth (d) is used to control mesh resolution (S) with a sigmoidal function as expressed in eq. 4 and (Fig. 1).

$$S = \frac{e^d}{e^d + 1}, \tag{4}$$

This decreases resolution from 521 m at 5 m depth and below to 5 km at around 400 m depth. Finally, bathymetric data from Beaman (2010) were linearly interpolated onto the mesh using HRDS (Hill, 2019).

2.3. Sediment transport

For the analysis of ooid grain formation, bed shear stress (BSS) is an important control on sediment movement generated by tidal currents in Thetis from the shallow water equation (eq. 1 and 2) (Martin-Short et al., 2015; Mitchell et al., 2010).

2.4. Simulation setup

Each of the five simulations used 11 tidal constituents (M2, S2, N2, K2, K1, O1, P1, Q1, M4, MS4, MN4) to represent astronomical tidal forcing. The forcing data were derived from TPXO (Egbert and Erofeeva, 2002) and used at the external/forced boundary only. Forcing data were applied via the boundary elevation and at each model timestep. Models were initially spun-up for 10 simulated days and then run for a further 30 simulated days to capture the spring-neap cycle. All analyses were done on the final 30 days of simulated tides. Each model used a timestep of 120 s with an output generated every 900 s. The wetting and drying parameter was $\alpha = 10.0$ to account for the steep slopes in places whilst maintaining numeric stability. Drag coefficient was set to 0.025. This avoids assumptions of locations of palaeo-reefs, which may have a higher drag coefficient, but still provides a good match in the modern to tidal gauge and FES2014 data (see below). A DIRK22 timestepping algorithm was used for temporal discretisation, as this has been shown to work well with the wetting and drying algorithm implemented in Thetis (Kärnä et al., 2018).

2.5. Model validation

To validate the Thetis simulation, a comparison with amplitude and

phase data was carried out against FES2014 data (Lyard et al., 2006), an independent tidal model which assimilates tide gauge data to provide the best match, similar to the TPXO data used to force the model.

3. Results

3.1. Model validation

The five tidal constituents M2, S2, K1, N2 and O1 were compared against FES2014 tidal observations. The tidal constituents with the best fit predicted by Thetis were M2 and S2 (standard error 1.3 cm, 3.3 cm), which are the most important and influential tidal constituents within the GBR lagoon. N2, O1 and K1 were also acceptable (standard error 3.8, 7.8 and 8.6 cm), as O1 and K1 are less important tidal constituents in the GBR, their higher SE values are acceptable for validation. All tidal constituent error measurements were statoistically significant (p< 0.01). These results are summarised in table 1 and the tidal gauge comparison in Fig. 3.

3.2. Morphological evolution of the Capricorn Channel system

Overall, we observe an increase in both tidal amplitude and tidal range as RSL rises and a reduction in bed shear stress within the Capricorn Channel over time (see Fig. 4 for modern bathymetry and dynamics). Changes to the bathymetry throughout the models (see Fig. 5 for all models) are as follows: the CC at 16.8 ka formed a 1–10 m deep inlet, 83 km long and 36 km wide and the coastline sits on the edge of the present continental shelf. At 15 ka the inlet is 5–35 m deep, 183 km long and 52 km wide; at 12.5 ka the inlet developed into a channel running between the coastline and the pre-Swain Reefs antecedent surface separating it from the Coral Sea. In this scenario water has to enter and leave the CC through the mouth or weave its way through the dense archipelago. There is a shallow shelf between the coastline and the continental edge. The depth of the CC mouth at this point ranges between 9 and 54 m. By 10 ka, RSL rose high enough (approximately −20 m below present-day RSL) to completely submerge the archipelago, allowing tidal water to leave and enter the CC by crossing the submerged archipelago and representing a closer fit to the present day southern GBR morphological setting. At this stage, depth of the CC mouth varies between 6 and 83 m. By the modern day, RSL has increased over the submerged archipelago, the GBR no longer acts as a buffer between the Coral Sea and the Queensland coast on the shallow shelf (Yokoyama et al., 2006). The depth of the CC mouth is now > 100 m deep.

3.3. Tidal dynamics and impact on bed shear stress

Here, we focus on the M2 and S2 tidal constituents. Maximum M2 amplitude levels have risen by over 190 cm (Fig. 6), particularly in the Herbert Creek area, in the last 16.8 ka. In the ooid area maximum M2 amplitude at 16.8 ka was ∼ 65 cm, which increased to around 100 cm at 15 ka rising to approximately 260 cm by present day. This increase in tidal amplitude develops at the same time as the development of the CC itself. Changes to the S2 amplitude follow the same pattern (Fig. 7): amplitude at 16.8 ka is relatively spatially uniform throughout the

Table 1

Tidal constituent validation statistics for each major tidal constituent. All constituents show a reasonable agreement to tidal gauge data and are statistically significant.

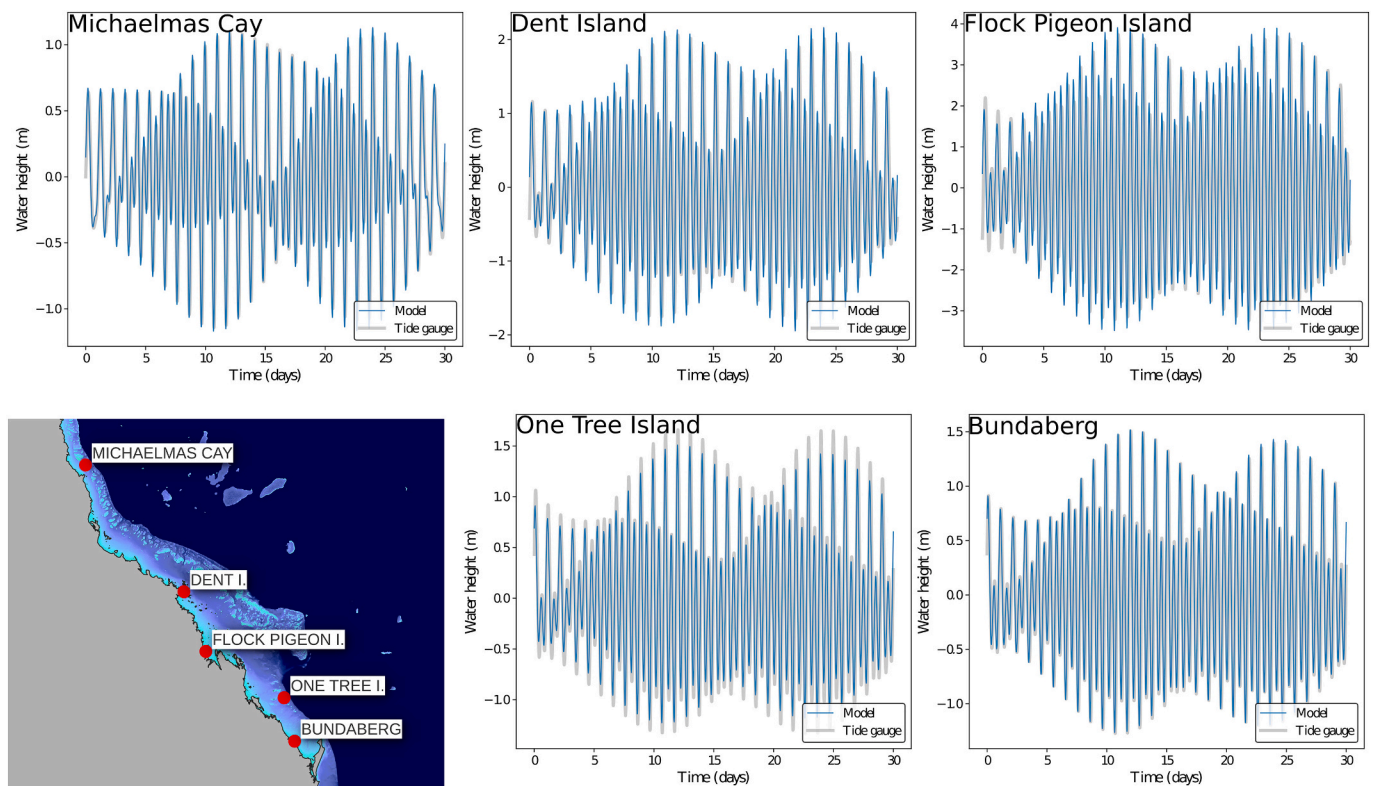| Constituent	r-value	P value	Standard error (m)
M2	0.993	< 0.01	0.013
S2	0.964	< 0.01	0.033
K1	0.878	< 0.01	0.078
O1	0.886	< 0.01	0.086
N2	0.951	< 0.01	0.038

Fig. 3. Tidal gauge data comparison between FES2014 and Thetis taken from locations of tidal gauges along Queensland coast.

whole domain at approximately 70 cm but becomes spatially varying across the time period with a maximum peak of 130 cm in the present day around Herbert Creek. Tidal range is dominated by M2 and therefore shows similar changes over the palaeo simulations (Fig. 8), the coast of Australia naturally experiences a much higher range of tidal range than the ooid area. At 16.8 ka, the ooid area experienced a maximum tidal range of 2.2 m, this tidal range has not changed to the present-day. This tidal range still allows constant agitation of the seabed. Along the coastline where tidal range is more greatly experienced, we found that the lowest tidal range of the palaeo simulations happens at 15 ka with values around half the tidal range of the modern GBR. Tidal range increase occurred after 10 ka, following the flooding of the GBR. This increase of tidal range has not been experienced in the ooid area. Average bed shear stress within the CC mouth was higher at 16.8 ka than at present day but BSS has increased in the ooid area since 16.8 ka as the CC developed. Max 16.8 ka BSS in the ooid area is mostly < 0.11 N/m^2 with some areas on the northern edge reaching > 0.47 N/m^2 (Fig. 9). It increases to mostly 0.110–0.194 N/m^2 at 15 ka, the same area in the present day has a max value of 0.194–0.27 N/m^2. At 16.8 ka, the BSS reaches those high levels within the open space of the inlet due to the tidal cycle creating eddies around small islands and particularly shallow areas with constant oscillation. The ooid area at 16.8 ka experiences very low BSS, an average of 0.11–0.194 N/m^2, this is lower than the necessary 0.27–0.47 N/m^2 for ooid formation.

3.4. Ooid forming conditions

Ooid grains require 0.27–0.47 N/m^2 to form, critical bed shear stress of >0.47 N/m^2 corresponds to the movement of coarse gravel as bedload; 0.27–0.47 N/m^2 corresponds to movement of coarse sand (Martin-Short et al., 2015). At 16.8 ka, the inlet is a very shallow shelf with water being funnelled through gaps around low lying land sitting at the mouth during low tide, at high tide the water submerges this land mass. At this point in time the inlet experiences maximum bed shear stress of >0.47

N/m^2 where two ooid samples were collected, however outside of the inlet, on the shelf where most of the ooid area is located, maximum BSS is $\sim$ 0.110–0.194 N/m^2. The average BSS within the inlet varies but large areas experience BSS greater than 0.27 N/m^2. Tidal range is very small at 16.8 ka, the furthest point of the inlet experiences $\sim$ 3 m tidal range whereas the ooid location experiences $\sim$ 1–2 m. At 15 ka, the channel mouth had physical conditions of a wide flat shelf which experienced maximum tidal velocity of 2 m/s, high tidal range of 5 m across a wide, long shelf with an average depth around 6 m (Table 1). These conditions enabled the production of average BSS of >0.47 N/m^2. In the present day, this same area is over 25 m deep, with a smaller tidal range of 1.5 m and a maximum tidal velocity of around 0.1 m/s.

Flow dynamics of tides through the CC have evolved alongside the bathymetric changes induced by RSL rise. At 16.8 ka flow dynamics were complicated by the low lying island obstructing the entrance. This funnelled water through two channels during low tide and during high tide the water flows over the submerged island. This makes oscillation complicated due to different depths and tidal flow restriction. At 15 ka, tides would have flowed in and out of the CC inlet freely, under this relative simple bathymetric setting tides would have oscillated back and forth (BSS of >0.47 N/m^2) with some complex flow patterns represented by eddy shedding (Fig. 10). Around 12.5 ka, the CC was bordering the paleo-coastline position and was sheltered by the dense archipelago on its northeastern flank. Dominant flows of water were directed northward from the mouth of the channel, with only some tidal flow coming in from the east through the archipelago or out of the main channel. Following the flood tide, the incoming flow would split into two directions: the northern half would continue north, up the channel, whereas the southern half would be pulled back out of the CC into the Coral Sea. This stage of CC development still experienced high levels of BSS (>0.47 N/m^2) with water flux being funnelled through the mouth of the channel and depth ranging between 59 and 9 m. By 10 ka, the archipelago is submerged and sees the emergence of the complex reef matrix that we have at present day, this allows tidal water to flow over
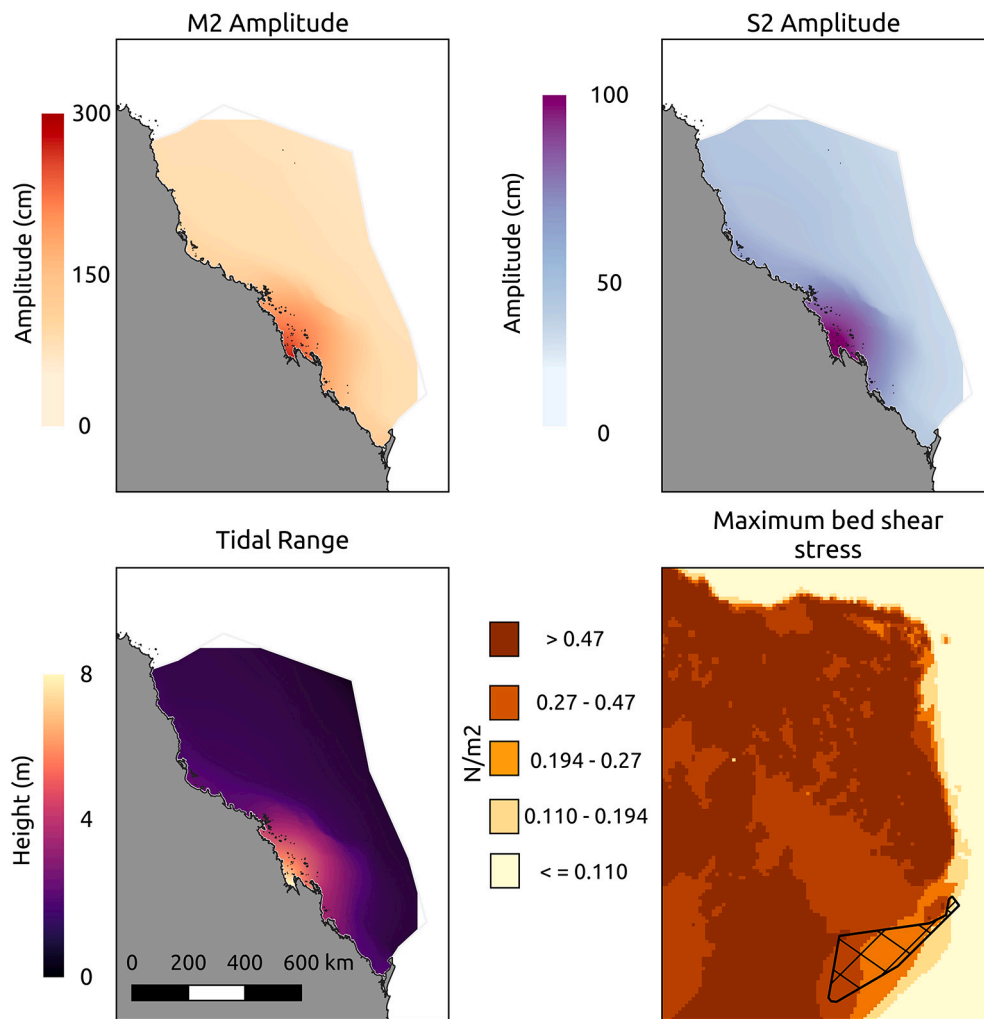
Fig. 4. Simulations of the modern domain to provide comparison against palaeo tidal amplitudes, tidal range for the whoel domain and bed shear stress around the Capricorn Channel. The hatched area in the bed shear stress map is that shown in Fig. 1 and is zoomed-in to show detail in the area of interest.
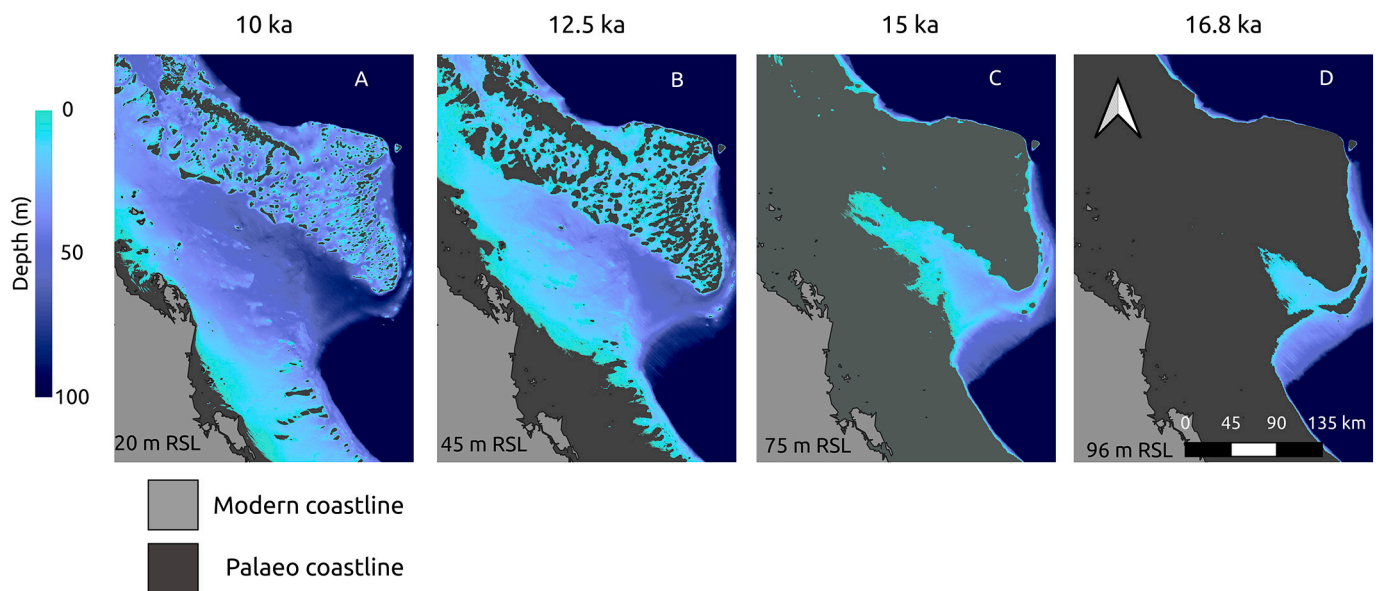

Fig. 5. Depth comparison over the palaeo simulations showing the effect relative sea level rise (Yokoyama et al., 2006) has had on the GBR bathymetry developed by Beaman (2010), accounting for the removal of Holocene reef growth.
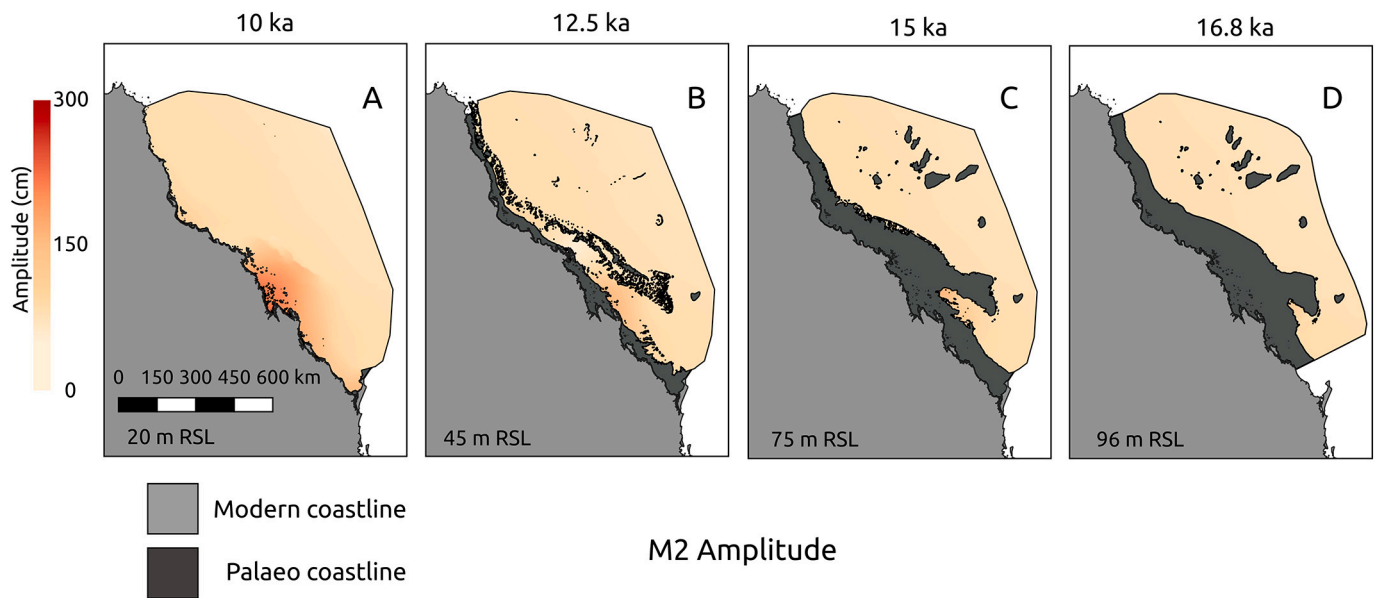
Fig. 6. Comparison of palaeo simulation results of M2 amplitude across the whole domain.
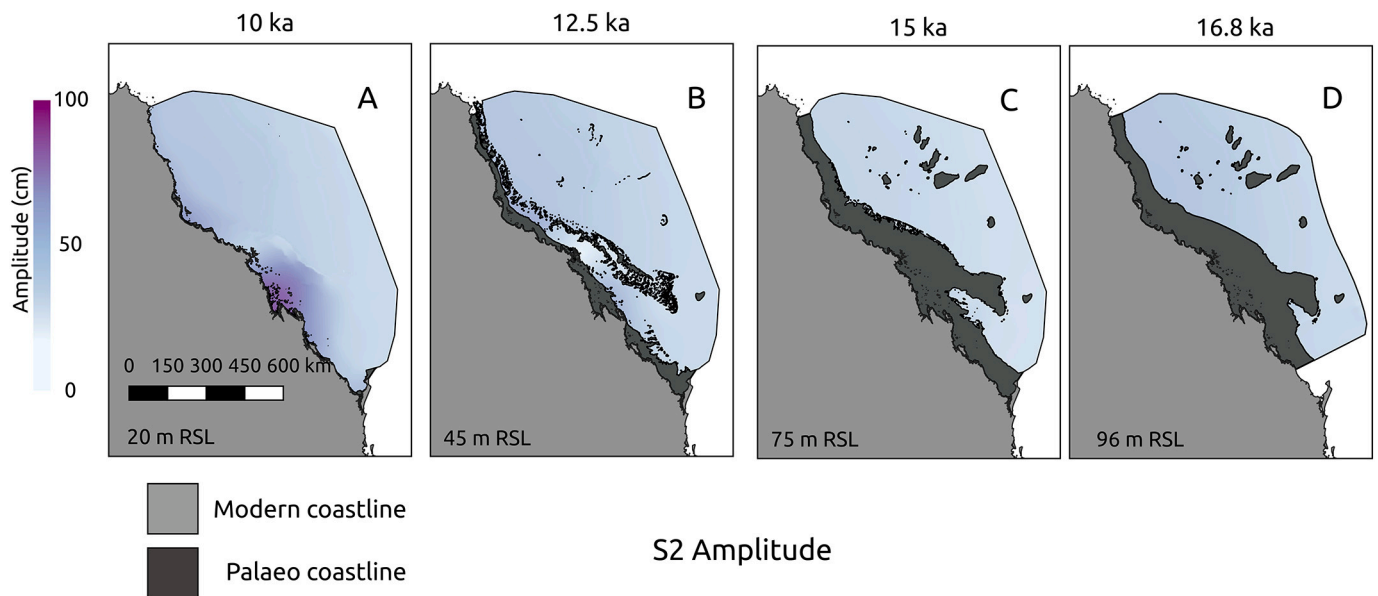

Fig. 7. Comparison of palaeo simulation results of S2 amplitude across the whole domain.

the reefs in and out of the CC as well as being funnelled through the channel mouth. At this stage the CC experiences a reduction of BSS due to increased depth and lower concentrations of tidal flow: in the present day the BSS is 0.27–0.47 N/m² and in 16.8 ka the BSS was >0.47 N/m² in the same location.

Overall, in the area of ooid formation, most tidal constituents have increased in amplitude as RSLs have risen, which, in turn, has increased tidal range through time. However, the BSS has generally decreased as RSLs have risen. The southern CC has seen more change over the past 16.8 ka than the northern CC has. At 16.8–15 ka, the conditions required for formation of ooid grains were present within the CC but not in the ooid area. These conditions disappeared by 12.5 ka as rising RSLs changed the water depth.

4. Discussion

4.1. Model limitations

The modelling work presented here is the first attempt to model the palaeo-tidal regime on the GBR. The simulations presented balance simulation cost, resolution and ensure proper representation of model dynamics. Previous work on the future RSL change on the GBR made similar compromises and showed good model performance with Thetis (Mawson et al., 2022). However, some limitations may affect the details presented, but not the main conclusions. Palaeo-reconstruction (palaeo-bathymetry and geomorphology) is a limitation on a large-scale study such as this. Previous modelling studies of palaeo-tides have made
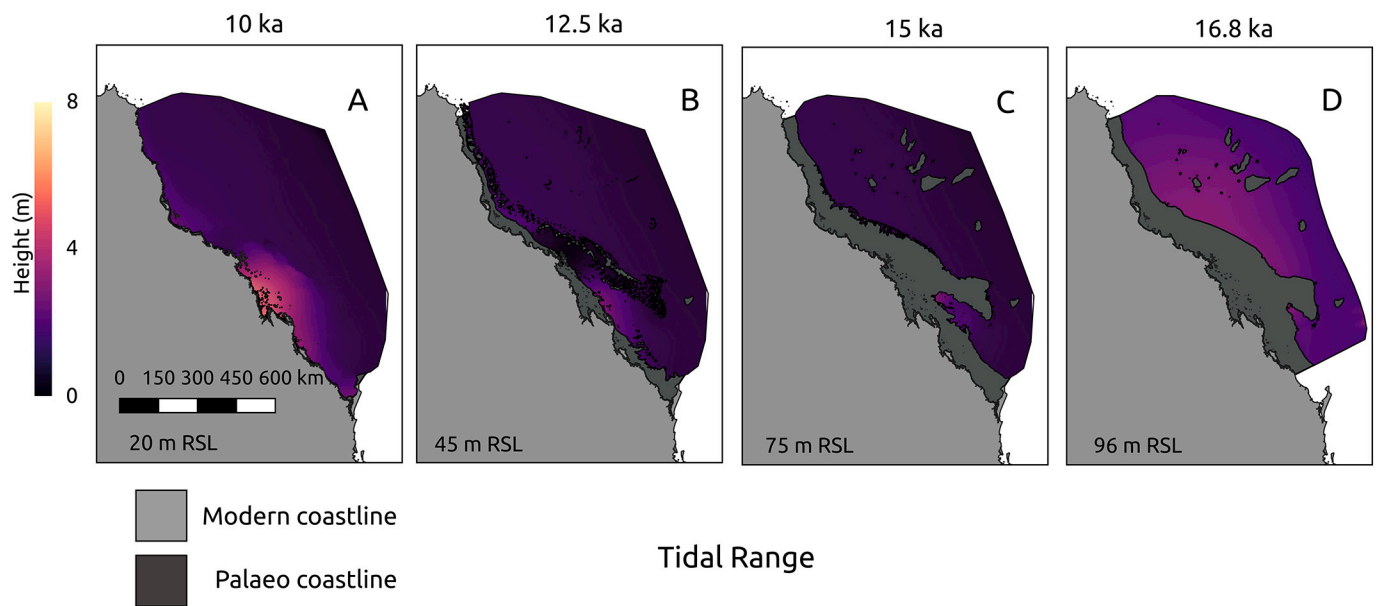
Fig. 8. Comparison of palaeo simulation results of tidal range across the whole domain.
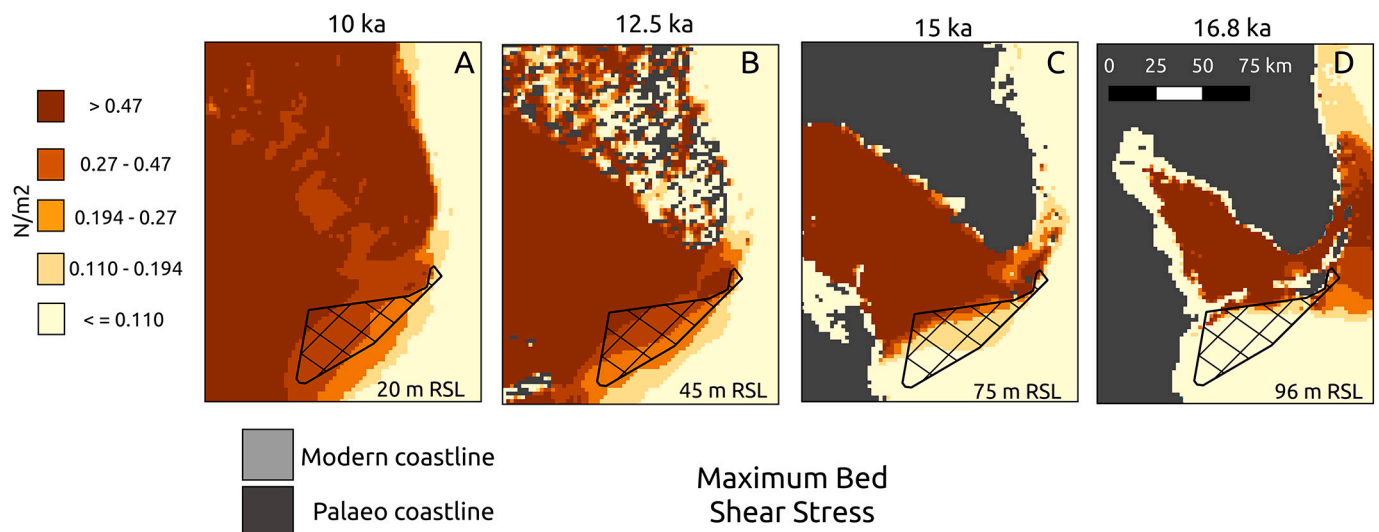

Fig. 9. Comparison of palaeo simulation results of maximum bed shear stress with particular attention to the area of ooid samples shown by polygon.

similar assumptions to those made here (Hinton, 1995; Shennan et al., 2000; Neill et al., 2010). However, studies such as this one are useful in guiding shoreline and shelf deposition processes (Collins et al., 2021). We have corrected for Holocene reef growth, but not for any geomorphological change over the last 16.8 ka. The minimum mesh resolution of 500 m could mean that very small bathymetric features are not resolved in the model. However, compared with the uncertainty of the palaeo-reconstruction we consider this limitation to be minor. We have used modern tidal forcing at the boundary throughout, global tides will have changed over the past 16.8 ka (Wilmes et al., 2017), however, there are no data available from global palaeo-tidal modelling studies that can be used in work such as the one presented here. As a further limitation to this model, wave action is not simulated despite wind driven waves often having a principal influence, alongside tidal flow, on the formation of ooids, particularly in areas such as the Bahamas (Rankey and Reeder, 2009). Due to the positioning of the CC mouth in 16.8 ka, it is likely that the ooid location was sheltered from waves driven across the Pacific. However, to fully assess the possible impact of wave induced current at 16.8 ka, one would need to carry out palaeo-climatic simulations to

assess possible wind-wave directions and strengths. It might then be possible to assess the combined impact of these processes to increase the temporal window in which odd grains could form; this is, however, beyond the scope of this study.

4.2. Tides have changed

The clear changes in bathymetry and RSL over the last 16.8 ka show that tidal processes have significantly changed, and the tidal processes seen at 16.8 ka no longer exist at present day. The key time period of substantial change was between 10 ka and 16.8 ka concomitant with glacial meltwater that caused the largest rise in RSL (Yokoyama et al., 2018). This increase in RSL ~10 ka caused the palaeo-surface around present-day Swain Reef area to be cut off from the mainland and transformed the CC from an inlet into a channel which ran over the entire length of the palaeo GBR. We found that this change could be responsible for the biggest shifts in tidal regimes around the GBR for the simulated period. Changes in the M2 and S2 amplitudes were primarily due to the bathymetric changes caused by rising RSLs. Tides originally
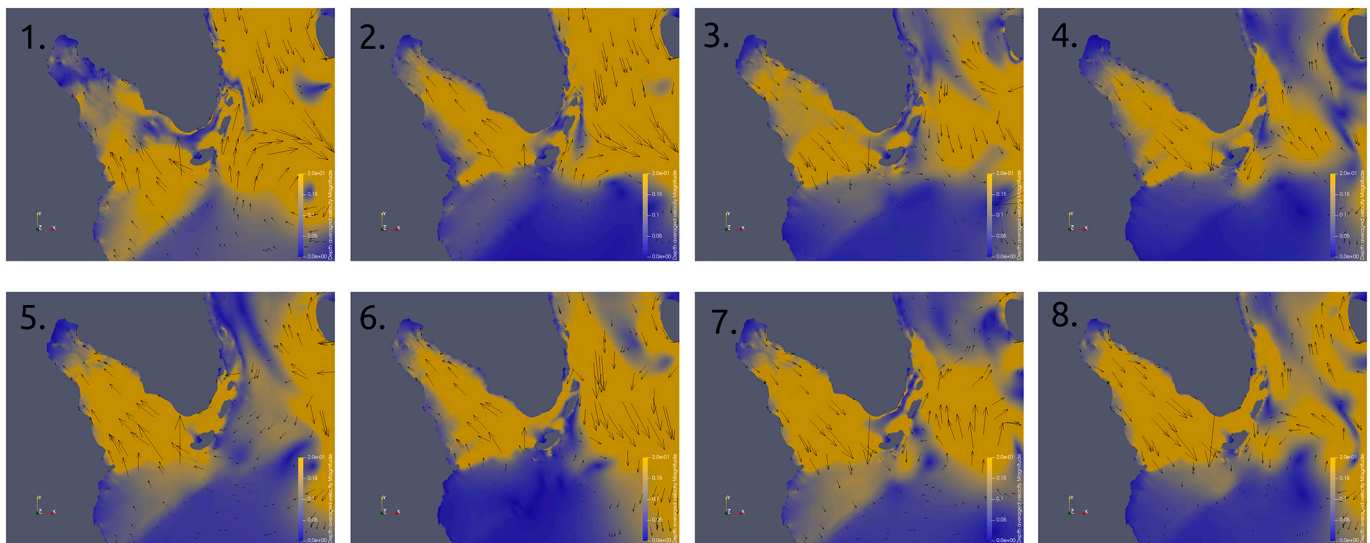
Fig. 10. Velocity vectors of 16.8 ka CC showing flow patterns across a 30 day period in equal intervals.

reached the palaeo-coastline without travelling across the continental shelf, whereas in the present day the tides cross the shelf 60–120 m deep and 200 km wide before reaching the coastline. Tides have also been changed by the presence of large areas of coral reef developed during the Holocene. The presence of reefs creates additional drag on the tidal flow, in turn this alters dynamics, primarily reducing velocity and affects tidal amplitudes and phases.

4.3. Ooid grain formation

The physical conditions required to support the original hypothesis of ooids forming in-situ are the following: tropical climate, increased and rapidly changing tidal currents on a wide, shallow, flat shelf and BSS of > 0.27 N/m^2 (Diaz and Eberli, 2019; Hearty et al., 2010; Szilagyi et al., 2020; Reeder and Rankey, 2008; Yokoyama et al., 2006). The modelling work presented here predicts all necessary conditions at 16.8 ka within the CC but not at the ooid sample area where the water is too deep (~30 m) to produce the necessary velocity and BSS, suggesting that majority of the ooids were not formed where they were found.

Within the CC, changes of tidal amplitude and tidal range in the CC suggest much lower tidal ranges than the present day. However, average velocity over a 30-day tidal cycle increased, suggesting faster and more energetic currents moving across the paleo-channel inlet between 16.8 and 12.5 ka. We found maximum velocity of 2 m/s corresponding to favourable conditions to move sediment up to 16 mm in diameter (Martin-Short et al., 2015). As ooid grains are 0.1–1.0 mm in diameter, a bed shear stress > 0.27 N/m^2, equivalent to a critical velocity of 0.275–0.701 m/s, is required to move them. Therefore, the simulated maximum velocity within the CC would be capable of creating the agitation claimed by Loreau and Purser (1973), eroding and agitating a large amount of sediment per tidal cycle. The mouth of the CC between 15 and 16.8 ka would likely have been suitable for forming ooid grains which have not yet been found.

The simulated maximum velocity within the ooid area would not have been capable of moving the ooid grains (0.05–0.1 m/s). However the ooid area is only 10 km away from an area which has very strong velocity (> 0.257 m/s) which could be capable of transporting ooids from the CC to where they were found.

Ooid grains formed in 2 m/s will be very fine compared to grains formed by the minimum 0.275 m/s (Rankey et al., 2006). As the ooids found in the CC are small (0.1–0.3 mm), they are more likely to have been formed in the high velocity environment 10 km away from the sample area and then moved to the area where they were found, this was

proposed as a hypothesis by Yokoyama et al. (2006). In a study by Hearty et al. (2010), ooids were found to have been transported downslope from where they had formed in Hawaii. The area where the ooids were found sits on a shelf that gradually slopes away from the CC down to the coral sea; it is highly likely that ooids formed in the mouth of the CC 10 km north of the ooid area before the tidal movement carried the ooids south down the slope. If RSL was dropped further, such as −120 m RSL, the ooids may have been able to form on the slope in a depth of 5 m. RSL 120 m below present would be a time period much further back (later than 24 ka) than when the ooid grains were estimated to be formed (Yokoyama et al., 2006). However, it has been proposed that the GBR ooid grains can been used to estimate past RSL. The work presented here means that this should be done with caution and with sufficient information on the likely formation locations and transport pathways of the sediments.

In the present day, the same high level of maximum velocity can be achieved along the CC in water 5 m deep, however the channel in these locations hosts dense coral reefs which restrict the open space required to form ooid grains and overwhelms the sediments Boyer (1972). The increased rate of velocity found in the palaeo CC inlet (2 m/s in 15 ka compared to 0.1 m/s in the present day) was most likely due to the northern channel being closed off, preventing water from leaving the channel by other routes and creating a circular system of tidal currents moving in and out of the same narrow opening. At 16.8 ka the CC mouth is a shallow bathymetry on a wide flat shelf, which is also required to produce ooids, whereas the ooid area in the present day is 25 m deep with a higher tidal range (Reeder and Rankey, 2008). The closed northern end of the CC in 16.8 ka made it possible for significant ooid grain formation to take place. The closure created an environment of high tidal range and sufficiently high velocity on a wide and shallow shelf in tropical waters. No samples were taken from within the CC where the inlet was, as ooid forming conditions were possible more may be found in that location. This is supported by two northern ooid sample locations being in areas of the necessary BSS. The finding of the inlet conditions also suggests ooids could have formed earlier than 16.8 ka, likely almost back to ~26 ka. Ooid formation time can vary depending on the conditions present, in the Great Salt Lake, ooids have been in the process of developing for the past 6000 years (Paradis et al., 2017), however ooids have also been created in lab conditions in a matter of weeks (Davies et al., 1978). The time window of ooid formation predicted by this study is 5000–6000 years. Short time frames of ooid forming conditions has been explored around the main Hawaiian islands following the finding of ooid grains which made been transported from

their place of formation, the time period was thought to be ~1900 yr before ceasing around 11.5 ka, this would be in alignment with Melt Water Pulse 1B which deepened the sea by 7.5 m at this time (Hearty et al., 2010; Webster et al., 2006). As the Hawaiian ooids were found to be similar to the ooids from the GBR, the short time frame of GBR ooid formation may too be tied to the Melt Water Pulse 1B.

5. Conclusion

Tidal dynamics on the GBR have dramatically changed over 16.8 ka in connection with 96 m of RSL rise and conditions which occurred during 16.8 ka no longer exist today. Only two of the seven dredge samples containing ooids were collected from sites where conditions could have supported the formation of ooids: BSS of >0.47 N/m^2, water depth of ~ 5 m, agitation from tidal range on a flat shelf. The other ooid samples were taken from sites which did not experience high enough levels of velocity and BSS to form, which suggests that the ooids formed within the CC inlet, where conditions were correct, and then transported down the sloping shelf to where they were found. As these ooids have been used to educate research on past RSLs, these RSLs could be incorrect as it was not expected that the ooid grains were transported to their location. The finding of ooid forming conditions being further north than the sample locations suggests that more ooids could be found in pipe dredge expeditions within the mouth of the CC. The period of time for ooid formation estimation from this study would be at least 5800 years between 11 ka and 16.8 ka. There is potential for ooid formation to go further back in time ~ 24 ka in line with past RSL predictions.

Data availability statement

All processed model output generated by this work can be found at https://doi.org/10.6084/m9.figshare.21400971.v1

Declaration of Competing Interest

The authors declare that they have no known competing financial interests or personal relationships that could have appeared to influence the work reported in this paper.

References

Andrews, J.C., Bode, L., 1988. The tides of the central great barrier reef. Cont. Shelf Res. 8, 1057–1085.

Andutta, F.P., Kingsford, M.J., Wolanski, E., 2012. 'Sticky water' enables the retention of larvae in a reef mosaic. Estuar. Coast. Shelf Sci. 101, 54–63.

Angeloudis, A., Kramer, S.C., Avdis, A., Piggott, M.D., 2018. Optimising tidal range power plant operation. Appl. Energy 212, 680–690.

Avdis, A., Candy, A.S., Hill, J., Kramer, S.C., Piggott, M.D., 2018. Efficient unstructured mesh generation for marine renewable energy applications. Renew. Energy 116, 842–856.

Beaman, R., 2010. Project 3DGBR: A high-resolution depth model for the great barrier reef and coral sea. Marine and Tropical Sciences Research Facility (MTSRF) Project 2.5i.1a Final Report. Reef and Rainforest Research Centre, Cairns, Australia, p. 13 plus Appendix 1.

Boyer, B.W., 1972. Grain accretion and related phenomena in unconsolidated surface sediments of the florida reef tract. J. Sediment. Res. 42, 205–210.

Collins, D.S., Avdis, A., Allison, P.A., Johnson, H.D., Hill, J., Piggott, M.D., Amir Hassan, M.H., Damit, A.R., 2017. Tidal dynamics and mangrove carbon

sequestration during the Oligo–Miocene in the south china sea. Nat. Commun. 8, ncomms15698.

Collins, D.S., Avdis, A., Wells, M.R., Dean, C.D., Mitchell, A.J., Allison, P.A., Johnson, H.D., Hampson, G.J., Hill, J., Piggott, M.D., 2021. Prediction of shoreline–shelf depositional process regime guided by palaeotidal modelling. Earth-Sci. Rev. 223, 103827.

Davies, P.J., Martin, K., 1976. Radial aragonite ooids, lizard island, great barrier reef, Queensland, Australia. Geology 4, 120–122.

Davies, P.J., Bubela, B., Ferguson, J., 1978. The formation of ooids. Sedimentology 25, 703–730.

Diaz, M.R., Eberli, G.P., 2019. Decoding the mechanism of formation in marine ooids: a review. Earth-Sci. Rev. 190, 536–556.

Egbert, G.D., Erofeeva, S.Y., 2002. Efficient inverse modeling of barotropic ocean tides. J. Atmos. Ocean. Technol. 19, 183–204.

Felis, T., Hinestrosa, G., Köhler, P., Webster, J.M., 2022. Role of the deglacial buildup of the great barrier reef for the global carbon cyle. Geophys. Res. Lett. 49.

Geuzaine, C., Remacle, J.F., 2009. Gmsh: a three-dimensional finite element mesh generator with built-in pre- and post-processing facilities. Int. J. Numer. Meth. Engng 0, 1–24.

Goss, Z., Warder, S., Angeloudis, A., Kramer, S., Avdis, A., Piggott, M., 2019. Tidal Modelling with Thetis: Preliminary English Channel Benchmarking.

Harker, A., Green, J.A.M., Schindelegger, M., Wilmes, S.B., 2019. The impact of sea-level rise on tidal characteristics around australia.

Hearty, P.J., Webster, J.M., Clague, D.A., Kaufman, D.S., Bright, J., Southon, J., Renema, W., 2010. A pulse of ooid formation in maui nui (hawaiian islands) during termination I. Mar. Geol. 268, 152–162.

Hill, J., 2019. HRDS: a python package for hierarchical raster datasets. JOSS 4, 1112.

Hinestrosa, G., Webster, J.M., Beaman, R.J., 2016. Postglacial sediment deposition along a mixed carbonate-siliciclastic margin: New constraints from the drowned shelf-edge reefs of the great barrier reef, Australia. Palaeogeogr. Palaeoclimatol. Palaeoecol. 446, 168–185.

Hinestrosa, G., Webster, J.M., Beaman, R.J., 2022. New constraints on the postglacial shallow-water carbonate accumulation in the great barrier reef. Sci. Rep. 12, 924.

Hinton, A.C., 1995. Holocene tides of the wash, U.K.: the influence of water-depth and coastline-shape changes on the record of sea-level change. Mar. Geol. 124, 87–111.

Hopley, D., Smithers, S.G., Parnell, K., 2007. The Geomorphology of the Great Barrier Reef: Development, Diversity and Change. Cambridge University Press, Cambridge, England.

Kärnä, T., Kramer, S.C., Mitchell, L., Ham, D.A., Piggott, M.D., Baptista, A.M., 2018. Thetis coastal ocean model: discontinuous galerkin discretization for the three-dimensional hydrostatic equations. Geosci. Model Dev. 11, 4359–4382.

King, B., Wolanski, E., 1996. Tidal current variability in the central great barrier reef. J. Mar. Syst. 9, 187–202.

Lambeck, K., Rouby, H., Purcell, A., Sun, Y., Sambridge, M., 2014. Sea level and global ice volumes from the last glacial maximum to the holocene. Proc. Natl. Acad. Sci. U. S. A. 111, 15296–15303.

Loreau, J.P., Purser, B.H., 1973. Distribution and ultrastructure of holocene ooids in the persian gulf. In: The Persian Gulf. Springer, Berlin Heidelberg, pp. 279–328.

Lyard, F., Lefevre, F., Letellier, T., Francis, O., 2006. Modelling the global ocean tides: modern insights from FES2004. Ocean Dyn. 56, 394–415.

Mackenzie, F.T., Pigott, J.D., 1981. Tectonic controls of phanerozoic sedimentary rock cycling. J. Geol. Soc. Lond. 138, 183–196.

Marshall, J.F., Davies, P.J., 1975. High-magnesium calcite ooids from the great barrier reef. J. Sediment. Res. 45, 285–291.

Marshall, J.F., Davies, P.J., 1984. Last interglacial reef growth beneath modern reefs in the southern great barrier reef. Nature 307, 44–46.

Martin-Short, R., Hill, J., Kramer, S.C., Avdis, A., Allison, P.A., Piggott, M.D., 2015. Tidal resource extraction in the pentland firth, UK: potential impacts on flow regime and sediment transport in the inner sound of stroma. Renew. Energy 76, 596–607.

Mawson, E.E., Lee, K.C., Hill, J., 2022. Sea level rise and the great barrier reef the future implications on reef tidal dynamics. J. Geophys. Res. C: Oceans 127.

Maxwell, W.G.H., Swinchatt, J.P., 1970. Great barrier reef: regional variation in a Terrigenous-Carbonate province. GSA Bull. 81, 691–724.

Mitchell, A.J., Uličný, D., Hampson, G.J., Allison, P.A., Gorman, G.J., Piggott, M.D., Wells, M.R., Pain, C.C., 2010. Modelling tidal current-induced bed shear stress and palaeocirculation in an epicontinental seaway: the Bohemian Cretaceous Basin, Central Europe. Sedimentology 57 (2), 359–388.

Neill, S.P., Scourse, J.D., Uehara, K., 2010. Evolution of bed shear stress distribution over the northwest european shelf seas during the last 12,000 years. Ocean Dyn. 60, 1139–1156.

Newell, N.D., Purdy, E.G., Imbrie, J., 1960. Bahamian Oölitic sand. J. Geol. 68, 481–497.

Paradis, O.P., Corsetti, F.A., Bardsley, A., Hammond, D.E., Xu, X., Walker, J.C., 2017. Radial ooids from great salt lake (Utah) as paleoenvironmental archives: Insights from radiocarbon chronology and stable isotopes. EP12A–06.

QGIS.org, 2020. QGIS Geographic Information System. QGIS Association. http://www.qgis.org.

Rankey, E.C., Reeder, S.L., 2009. Holocene ooids of Aitutaki Atoll, Cook Islands, South Pacific. Geology 37, 971–974. https://doi.org/10.1130/G30332A.1.

Rankey, E.C., Riegl, B., Steffen, K., 2006. Form, function and feedbacks in a tidally dominated ooid shoal, Bahamas. Sedimentology 53, 1191–1210.

Reeder, S.L., Rankey, E.C., 2008. Interactions between tidal flows and ooid shoals, northern Bahamas. J. Sediment. Res. 78, 175–186.

Salles, T., Pall, J., Webster, J.M., Dechnik, B., 2018. Exploring coral reef responses to millennial-scale climatic forcings: insights from the 1-D numerical tool pyReef-Core v1.0. Geosci. Model Dev. 11, 2093–2110.

Seifi, F., Deng, X., Baltazar Andersen, O., 2019. UoNGBR: a regional assimilation barotropic tidal model for the great barrier reef and coral sea based on satellite, coastal and marine data. Remote Sens. 11, 2234.

Shennan, I., Lambeck, K., Flather, R., Horton, B., McArthur, J., Innes, J., Lloyd, J., Rutherford, M., Wingfield, R., 2000. Modelling western north sea palaeogeographies and tidal changes during the holocene. Geol. Soc. Lond., Spec. Publ. 166, 299–319.

Simone, L., 1980. Ooids: a review. Earth-Sci. Rev. 16, 319–355.

Szilagyi, Z., Webster, J.M., Patterson, M.A., Hips, K., Riding, R., Foley, M., Humblet, M., Yokoyama, Y., Liang, L., Gischler, E., Montaggioni, L., Gherardi, D., Braga, J.C., 2020. Controls on the spatio-temporal distribution of microbialite crusts on the great barrier reef over the past 30,000 years. Mar. Geol. 429, 106312.

Taebi, S., Lowe, R.J., Pattiaratchi, C.B., Ivey, G.N., Symonds, G., Brinkman, R., 2011. Nearshore circulation in a tropical fringing reef system. J. Geophys. Res. 116, 40.

Taylor, J.C.M., Illing, L.V., 1969. Holocene intertidal calcium carbonate cementation, Qatar, Persian Gulf. Sedimentology 12, 69–107.

Webster, J.M., Davies, P.J., 2003. Coral variation in two deep drill cores: significance for the pleistocene development of the great barrier reef. Sediment. Geol. 159, 61–80.

Webster, J.M., Clague, D.A., Braga, J.C., Spalding, H., Renema, W., Kelley, C., Applegate, B., Smith, J.R., Paull, C.K., Moore, J.G., Potts, D., 2006. Drowned coralline algal dominated deposits off lanai, Hawaii; carbonate accretion and vertical tectonics over the last 30 ka. Mar. Geol. 225, 223–246.

Webster, J.M., Braga, J.C., Humblet, M., Potts, D.C., Iryu, Y., Yokoyama, Y., Fujita, K., Bourillot, R., Esat, T.M., Fallon, S., Thompson, W.G., Thomas, A.L., Kan, H., McGregor, H.V., Hinestrosa, G., Obrochta, S.P., Lougheed, B.C., 2018. Response of the great barrier reef to sea-level and environmental changes over the past 30,000 years. Nat. Geosci. 11, 426–432.

Wilmes, S.B., Green, J.A.M., Gomez, N., Rippeth, T.P., Lau, H., 2017. Global tidal impacts of large-scale ice sheet collapses. Journal of Geophysical Research: Oceans 122, 8354–8370.

Wolanski, E., 1983. Tides on the northern great barrier reef continental shelf. J. Geophys. Res. 88, 5953.

Yokoyama, Y., Purcell, A., Marshall, J.F., Lambeck, K., 2006. Sea-level during the early deglaciation period in the great barrier reef, Australia. Glob. Planet. Chang. 53, 147–153.

Yokoyama, Y., Esat, T.M., Thompson, W.G., Thomas, A.L., Webster, J.M., Miyairi, Y., Sawada, C., Aze, T., Matsuzaki, H., Okuno, J., Fallon, S., Braga, J.C., Humblet, M., Iryu, Y., Potts, D.C., Fujita, K., Suzuki, A., Kan, H., 2018. Rapid glaciation and a two-step sea level plunge into the last glacial maximum. Nature 559, 603–607.